AIP Applied Physics Letters

Aberration-free and functionality-switchable meta-lenses based on tunable metasurfaces

He-Xiu Xu, Shaojie Ma, Weijie Luo, Tong Cai, Shulin Sun, Qiong He, and Lei Zhou

Citation: Applied Physics Letters **109**, 193506 (2016); doi: 10.1063/1.4967438
View online: http://dx.doi.org/10.1063/1.4967438
View Table of Contents: http://scitation.aip.org/content/aip/journal/apl/109/19?ver=pdfcov
Published by the AIP Publishing

Aberration-free and functionality-switchable meta-lenses based on tunable metasurfaces

He-Xiu Xu,[1,2,a)] Shaojie Ma,[1] Weijie Luo,[1] Tong Cai,[1,2] Shulin Sun,[3] Qiong He,[1,4] and Lei Zhou[1,4,a)]
[1]*State Key Laboratory of Surface Physics, Key Laboratory of Micro and Nano Photonic Structures (Ministry of Education) and Physics Department, Fudan University, Shanghai 200433, China*
[2]*Air and Missile Defense College, Air Force Engineering University, Xi'an 710051, China*
[3]*Shanghai Engineering Research Center of Ultra-Precision Optical Manufacturing, Green Photonics and Department of Optical Science and Engineering, Fudan University, Shanghai 200433, China*
[4]*Collaborative Innovation Center of Advanced Microstructures, Nanjing 210093, China*

(Received 20 August 2016; accepted 27 October 2016; published online 11 November 2016)

Constructing a meta-lens with tunable meta-atoms with varactor diodes incorporated, we can precisely control the phase profile of the meta-lens by varying the external voltages imparted on the diodes, such that the dispersion-induced phase distortions at off-working frequencies can be rectified and the functionality of the meta-lens can be dynamically changed. As an illustration, we design and fabricate a tunable meta-lens in the microwave regime and employ both experiments and numerical simulations to demonstrate the aberration-free and dynamically switchable focusing performances of the meta-lens. Our approach paves the road to achieve dispersion-corrected and switchable manipulations of electromagnetic waves in the microwave regime. *Published by AIP Publishing.*
[http://dx.doi.org/10.1063/1.4967438]

Controlling the abrupt phase distributions on metasurfaces (planar inhomogeneous metamaterials constructed by meta-atoms with tailored electromagnetic (EM) properties) have led to fascinating effects such as anomalous light refraction/reflection,[1–12] propagating wave to surface wave coupling,[13,14] flat-lens focusing,[15–24] holograms,[25–28] optics-vortex generation,[29] polarization control,[30,31] and photonic spin-Hall effect.[32,33] To design these metasurfaces with certain functionalities, one typically combines a set of resonant meta-atoms with distinct EM responses to form a planar structure, such that the whole device exhibits the desired profile of transmission/reflection amplitude/phase. However, such a designing strategy only works for a *single* frequency, since the desired phase profile cannot maintain at other frequencies due to the intrinsic dispersions of passive resonant meta-atoms.[1–33] Such *intrinsic dispersions* limit the working bandwidths and functionalities of passive meta-devices realized so far, since their performances quickly get deteriorated at frequencies other than the target frequency, and their functionalities cannot be changed once they are fabricated. Such an issue seems inherent to all metasurfaces based on *passive* resonant meta-atoms, working in either reflection or transmission geometries and relying on either phase or amplitude modulations,[34,35] and cannot be completely solved by conventional bandwidth-expansion methods using low-Q and/or multi-mode resonators.[7–11]

In this letter, we establish an active scheme to overcome such dispersion-induced issues. By making *tunable* metasurfaces with all individual meta-atoms independently controlled by external knobs, we can *precisely* control the phase profiles of the metasurfaces at different frequencies, so that not only the dispersion-induced phase distortions can be rectified but also the functionalities of the meta-devices can be dynamically switched. Based on such a scheme, we *experimentally* demonstrated two active meta-lenses, one exhibiting the *same* focal point for *all* frequencies laying a wide band while the other enables dynamically switched imaging functionalities. For both devices, numerical simulations are in excellent agreement with near-field scanning experiments, demonstrating the validity of the proposed active scheme. Our approach allows dynamical controls on the EM functionalities of *inhomogeneous* metasurfaces focusing particularly on solving the *dispersion-induced* issues, distinct from previous efforts on using varactors/diodes to tune the resonant frequencies,[36] EM wave-fronts,[37–40] and transmission/reflection properties[41] of metasurfaces with limited frequency-tuning ranges.

We first describe our strategy to design the tunable meta-atoms. To facilitate our further designs of the meta-lenses, we adopt those meta-atoms exhibiting relatively large frequency/phase tuning range and nearly uniform reflection magnitudes. Based on these considerations, we chose a two-mode reflective-type meta-atom with geometrical details shown in Fig. 1(a). Specifically, our meta-atom is a tri-layer structure consisting of a composite planar resonator (containing a metallic "H" structure and a metallic patch) coupled with a metallic ground plane through a dielectric spacer ($\varepsilon_r = 2.65$, $h = 6$ mm, and loss tangent $\tan\delta = 0.001$). The couplings between the top structure and the ground plane generate two magnetic resonances at frequencies f_1 and f_2, evidenced by the dips in the finite-difference-time-domain (FDTD) simulated x-polarized reflection spectrum depicted in Fig. 1(b). Cascading the two resonances appropriately makes our meta-atom exhibit a much enlarged working bandwidth (2–7 GHz, see solid lines in Fig. 1(b)). To make the meta-atom tunable, we break the central bar of the "H" structure and then connect its two parts by a varactor diode (SMV1430-079LF, Skyworks Solutions Inc.[42]), which is then controlled by an external voltage source.

[a)]Authors to whom correspondence should be addressed. Electronic addresses: phzhou@fudan.edu.cn and hxxuellen@gmail.com

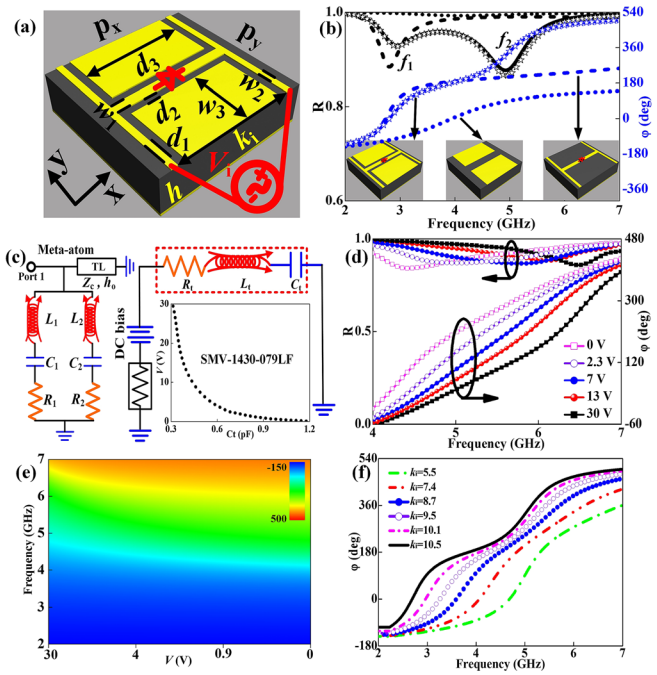

FIG. 1. (a) Geometry of the basic meta-atom. (b) FDTD (lines) and CM (stars) -simulated spectra of reflectance (black curves, left axis) and reflection-phase (blue curves, right axis) of three periodic metasurfaces with unit-cells being the composite meta-atom (solid lines), meta-atom with patch only (dotted lines), and meta-atom with "H" only (dashed lines), with the capacitance of the varactor diode fixed as $C_t = 0.6$ pF corresponding a fixed biasing voltage 4 V. Here, $k_i = 10.5$ mm. (c) The equivalent CM for the tunable meta-atom and the varactor diode SMV1430-079LF with inset depicting its C_t-V curve. (d) FDTD simulated spectra of reflectance and reflection phase of a metasurface consisting of a periodic array of meta-atoms with $k_i = 7.4$ mm, under different biasing voltages. (e) FDTD simulated reflection-phase as a function of biasing voltage V and frequency for the same system studied in (d). (f) FDTD calculated reflection-phase spectra of periodic metasurfaces with different parameter k_i. The geometrical parameters of the meta-atoms are fixed as $p_x = p_y = 12$ mm, $w_1 = 0.8$ mm, $w_2 = 0.5$ mm, $w_3 = 5.1$ mm, $d_1 = 0.25$ mm, and $d_2 = 0.5$ mm. The circuit parameters in our CM calculations for (b) are $L_1 = 19$ nH, $C_1 = 0.085$ pF, $L_2 = 0.09$ nH, $C_2 = 0.194$ pF, $R_1 = 4.22\ \Omega$, $R_2 = 0.37\ \Omega$, $Z_c = 207.4\ \Omega$, and $h_o = 58.9°$; here, Z_c and h_o in CM are the equivalent impedance and electrical length modeling the transmission through the dielectric spacer.

The physical principle of the tunability can be understood from the equivalent circuit model (CM) of the entire system as shown in Fig. 1(c), where two magnetic resonances at f_1 and f_2 are modeled by two series resonant tanks formed by L_1, C_1 and R_1, and L_2, C_2 and R_2, respectively. These lumped circuit parameters, contributed from different parts of the composite resonator as well as the varactor diode (see Fig. 1(c)), are finally retrieved from the corresponding FDTD simulated spectra on realistic structures. In our FDTD simulations, we replaced the varactor diode by a series resonant tank with inductance $L_t = 0.7$ nH, resistance $R_t = 1.5\ \Omega$, and capacitance C_t, which sensitively depends on the voltage V imparted on it through a $C_t \sim V$ curve depicted in the inset to Fig. 1(c). The established CM is justified by the excellent agreement between the results based on FDTD simulations and the CM (see stars in Fig. 1(b)). The physics of the varactor-enabled tunability is thus clear: varying the external voltage V can modify the capacitance C_t of the diode, which, in turn, tunes the frequencies (particularly f_1) of the two resonant modes through modifying their effective capacitances C_1 and C_2, and thus the related reflection-phase spectra.

Figure 1(d) compares the FDTD simulated reflection spectra of a metasurface consisting of a *periodic* array of such tunable meta-atoms, which are simultaneously biased at the same voltage V varying from 0 to 30 V. Indeed, the resonant mode f_1 varies sensitively as a function of V, leading to a dramatic tuning of the reflection phases.[43] However, the reflectance R remains nearly 90% since this is a reflective meta-atom with a continuous metal ground plane and the loss is very small in the microwave regime. Figure 1(e) depicts how the reflection phase φ of the studied tunable meta-atom varies as a function of frequency and the biasing voltage. For every frequency inside the band (4–7 GHz), one can always get a large tuning range of φ (covering more than 175° at ~5.7 GHz), which provides a large freedom to design our meta-lens.

With the EM properties of the tunable meta-atoms fully understood, we start to design our meta-lenses employing such meta-atoms. Restricted by the geometries of our meta-atoms, we can only realize one-dimensional *tunable* lens where a column of meta-atoms are controlled by the *same* voltage source. Two-dimensional tunable lens needs sophisticated designs on both the meta-atoms and the control circuits. We assume that our meta-lenses exhibit the following parabolic reflection-phase profiles:

$$\varphi(x,f) - \varphi(0,f) = -\frac{2\pi}{\lambda}\left(\sqrt{x^2 + F^2} - F\right), \qquad (1)$$

where x denotes the position of the meta-atom and $\varphi(0,f)$ is the reflection phase at the lens center. Here, f and λ are the working frequency and wavelength while F is the designed focal length. We choose 6 different types of tunable meta-atoms (labeled by 1, 2, 3, 4, 5, and 6) to design our meta-lenses, and each vertical row of meta-atoms (all having the same structure) is controlled by an external voltage source (see Fig. 2(a)).

As a starting point, we first design a meta-lens exhibiting the phase profile described by Eq. (1) with $F = 60$ mm at $f = 5.5$ GHz, using 6 different types of meta-atoms but under *zero* biasing voltages ($V_i = 0, i = 1, ..., 6$ and thus $C_t = 1.2$ pF). Without involving too many complications, in our design we only vary the width of the patch resonator (denoted by k_i for the ith meta-atom) but keeping other geometrical parameters unchanged. Figure 1(f) depicts how the reflection-phase spectrum of our meta-atom varies as its k_i changes. The parameters $\{k_i\}$ were found as 5.5, 7.4, 8.7, 9.5, 10.1, and 10.5 mm, respectively, which can help yield the desired $\varphi(x)$ profile (215.1°, 273.4°, 325.9°, 371.8°, 406.9°, and 429.5°) at $f = 5.5$ GHz. Meanwhile, the reflection amplitudes of all meta-atoms are larger than 0.9 with fluctuations less than 0.1. With the geometrical parameters of these meta-atoms fixed, we then employed FDTD simulations to calculate the $\varphi_i(f) \sim V_i$ relationships for all six meta-atoms (similar to Figs. 1(d) and 1(e), not shown here). Based on these complete information, we thus retrieved the voltages $\{V_i\}$ imparted on the diodes involved in different meta-atoms employing a root-finding algorithm called traversal query, requiring the meta-lens to exhibit the desired phase profile (Eq. (1)) with a pre-determined focal length F at an arbitrary frequency f. The solutions of $\{V_i\}$ depend

sensitively on the values of F and f. Since the $\{V_i\}$ solution yielding a desired phase distribution may not be unique, we selected the solution that exhibits the minimum variation on C_t of 6 meta-atoms at each frequency.

To clearly see the dispersion-induced issues in *passive* meta-lenses, we purposely choose a structure with a *fixed* $\{V_i\}$ to *mimic* a passive meta-lens. Without losing generality, here we choose the solution of $\{V_i\}$ obtained for $F = 75$ mm at $f = 5.5$ GHz. Figure 2(c) presents the focusing performances of such a meta-lens at different frequencies. As expected, at $f = 5.5$ GHz the lens does exhibit a perfect focusing performance with a clear focal point at $F = 75$ mm, identified as the peak-field position along the optical axis (see Fig. 5(c)), which is also the position below/above which the EM wavefront is of a concave/convex shape.[44,45] However, at frequencies other than 5.5 GHz, either the focal point deviates from $F = 75$ mm (5.8, 6.1, and 6.4 GHz) or the focusing performances become bad (4.9, 5.2 GHz), showing that a passive meta-lens exhibits clear chromatic aberrations. The underlying physics is very clear. For such a *passive* meta-lens, the intrinsic dispersions of meta-atoms make the phase profiles of the meta-lens deviate quickly from the ideal solution Eq. (1), at frequencies other than the target one 5.5 GHz (see Fig. 2(b)).

Such issue can be solved once we dynamically tune $\{V_i\}$ to rectify the distorted phases and thus make Eq. (1) satisfied at *arbitrary* frequencies. We retrieved the requested voltages $\{V_i\}$ at arbitrary frequencies by requiring the resulting $\varphi(x)$ to satisfy Eq. (1) with $F = 75$ mm. Figure 3(a) depicts the obtained $V_i \sim f$ curves, which are necessary to correct the otherwise distorted phase distributions (see Fig. 3(b) for $\varphi_i \sim f$ curves under such biasing voltages). As a result, at an arbitrary frequency within the working band, our meta-lens can *always* exhibit the *correct* $\varphi(x)$ satisfying Eq. (1) (see the inset to Fig. 3(b) for an example at 5.9 GHz). Under these biasing voltages, our meta-lens must be free of aberrations since it can always exhibit perfect phase profiles.

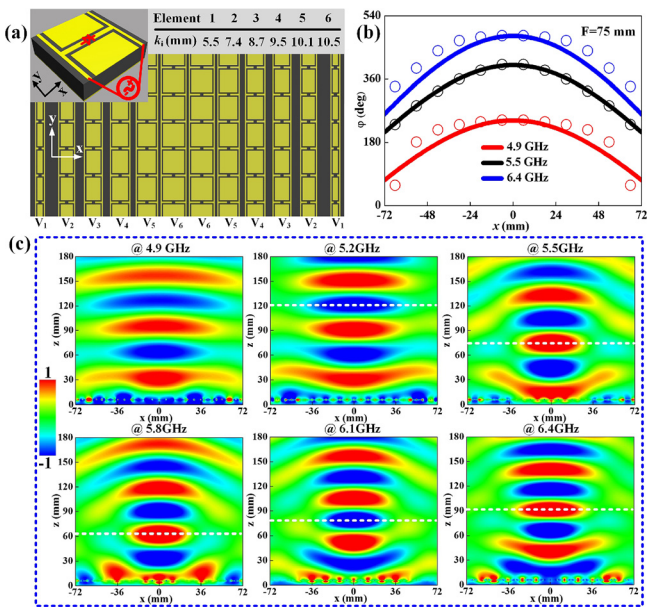

FIG. 2. (a) Geometry of the designed meta-lens composed by 12×9 meta-atoms. The lens exhibits a $x \rightarrow -x$ mirror symmetry and is formed by six different types of meta-atoms with parameters $k_i = 5.5$, 7.4, 8.7, 9.5, 10.1, and 10.5 mm. (b) $\varphi(x)$ profiles of the *passive* meta-lens at three different frequencies, obtained by FDTD simulations (symbols) and Eq. (1) (lines). (c) FDTD simulated Re(E_x) field distributions of the *passive* meta-lens at different frequencies, when the meta-lens is illuminated by an x-polarized plane wave. The incident field is deducted from the total field. The *passive* lens is taken as the meta-lens under *fixed* biasing voltages corresponding to $F = 75$ mm and $f = 5.5$ GHz.

We can further design a functionality-tunable meta-lens utilizing the same approach. Set the working frequency at 5.5 GHz, we retrieved the requested biasing voltages $\{V_i\}$ for the same meta-lens by requiring that its focal length F changes from 45 mm to 120 mm. Figure 3(c) depicts the obtained $\{V_i\}$ as a function of the designed focal length F. As expected, we have $\{V_i = 0\}$ for $F = 60$ mm, which is the starting point of our design. Figure 3(d) shows how the resultant reflection amplitudes/phases of six meta-atoms vary against F under the voltage combinations $\{V_i\}$ as depicted in Fig. 3(c). Under the biasing voltages given in Fig. 3(c), our active meta-lens thus behaves as a functionality-switchable device with tunable focal length.

We fabricated a realistic sample according to the design and experimentally characterized all the predicted properties (i.e., aberration-free and functionality-switchable imaging). The sample was fabricated based on the printed-circuit-board technique, with an overall size of 144×108 mm^2 (see Fig. 4(a) for its top-view picture). All varactor diodes were attached to the top metallic microstructure using surface-mount technology, which are then biased by appropriate constant-voltage sources (GPD4303S, GWINSTEK company, Taiwan). To experimentally test the focusing properties of our meta-lens, we shine the meta-lens (under appropriate biasing voltages as given in Figs. 3(a) and 3(c)) by x-polarized plane waves emitted from a horn antenna placed at 900 mm away from the meta-lens, and then used a 15 mm-long monopole antenna to measure the distributions of local E_x field (with both amplitude and phase) on the xz plane. To see the focusing properties clearly, we purposely deducted the incident field from the measured data so that only the scattered fields are presented.

Figure 4 depicts the measured Re(E_x) distributions for our meta-lens under two different groups of biasing voltages as recorded in Figs. 3(a) and 3(c). As expected, under the biasing voltages as shown in Fig. 3(a), the meta-lens can always focus incident waves to the focal point at $F = 75$ mm, no matter how we vary the working frequency (see Fig. 4(c)). Such an aberration-free imaging property is in sharp contrast to the passive meta-lens as described in Fig. 2(c). Meanwhile, keeping the working frequency at 5.5 GHz and adopting the other group of biasing voltages presented in Fig. 3(c), we found that our meta-lens can exhibit excellent focusing functionalities, but with the focal point switched dynamically from 45 to 120 mm as we change the biasing voltages appropriately. The intrinsic physics underlying these interesting effects is again that our meta-lens can exhibit the desired (undistorted) phase profiles, under appropriate biasing voltages (see Fig. 4(b)).

The aberration-free and functionality-switchable focusing properties of our meta-lens are finally verified by FDTD simulations. Figure 5 plots the corresponding FDTD simulated Re(E_x) distributions of the meta-lens, under two different biasing voltages as shown in Figs. 3(a) and 3(c). Perfect

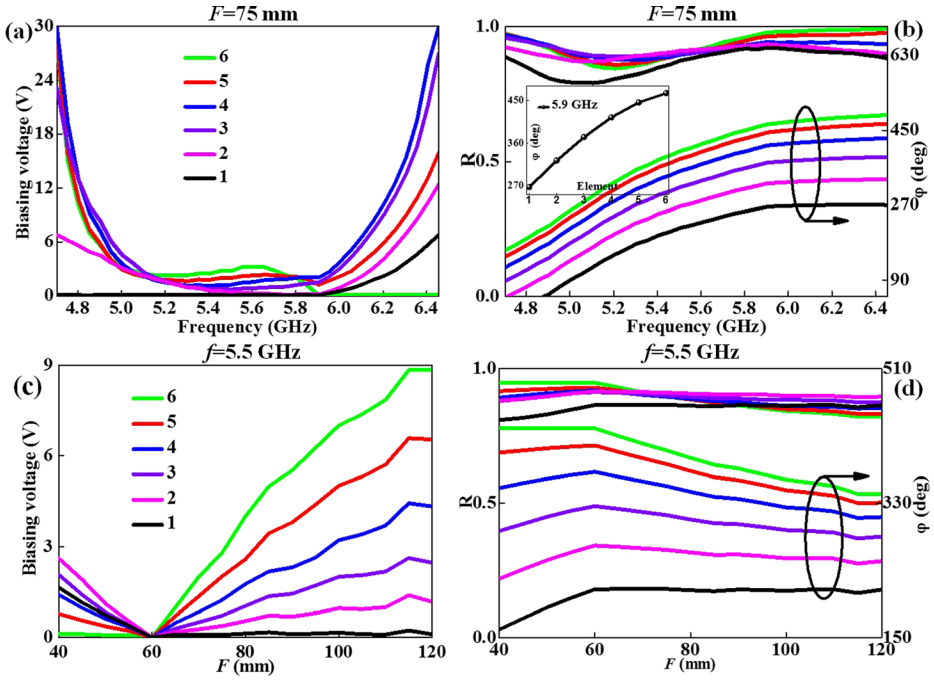

FIG. 3. (a) Retrieved voltages $\{V_i\}$ and (b) FDTD calculated reflection coefficients (R and φ) of six meta-atoms as functions of frequency for the designed aberration-free lens with $F = 75$ mm. (c) Retrieved voltages $\{V_i\}$ and (d) FDTD calculated reflection coefficients (R and φ) of six meta-atoms as a function of the desired focal length F for the functionality-switchable lens working at 5.5 GHz. Inset to (b) shows the phase profile of the meta-lens under the biasing voltages in (a) for $f = 5.9$ GHz.

focusing effects of the meta-lens are observed for all the cases studied, which are in good agreement with their corresponding experimental results. In particular, Fig. 5(a) shows that the performance of our meta-lens can be free of aberrations while Fig. 5(b) shows that its focal lens can be dynamically switched. The good agreement between theory and experiment is clearly shown in Figs. 5(c)–5(f), where the measured and simulated field distributions along the optical z axis (with x = 0 mm) and the focal line are compared in two particular cases studied. As expected, **E** field intensity

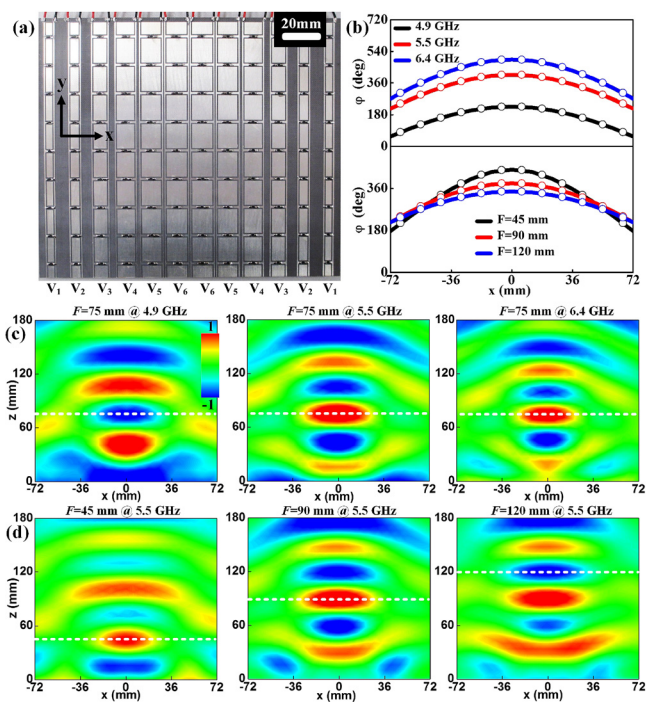

FIG. 4. (a) Picture of the fabricated sample. (b) $\varphi(x)$ for the aberration-free lens with $F = 75$ mm at three frequencies (top panel), and for the functionality-switchable lens with different focal points ($F = 45$, 90, and 120 mm) at 5.5 GHz (bottom panel), obtained by FDTD simulations on our tunable lenses (symbols) and Eq. (1) (lines). Experimentally measured Re(E_x) distributions for (c) the aberration-free lens with $F = 75$ mm at 4.9, 5.5, and 6.4 GHz, respectively, and (d) the functionality-switchable lens with $F = 45$, 90, and 120 mm at 5.5 GHz. The incident field has been eliminated from the measured field. While dashed lines denote the positions of the focal plane.

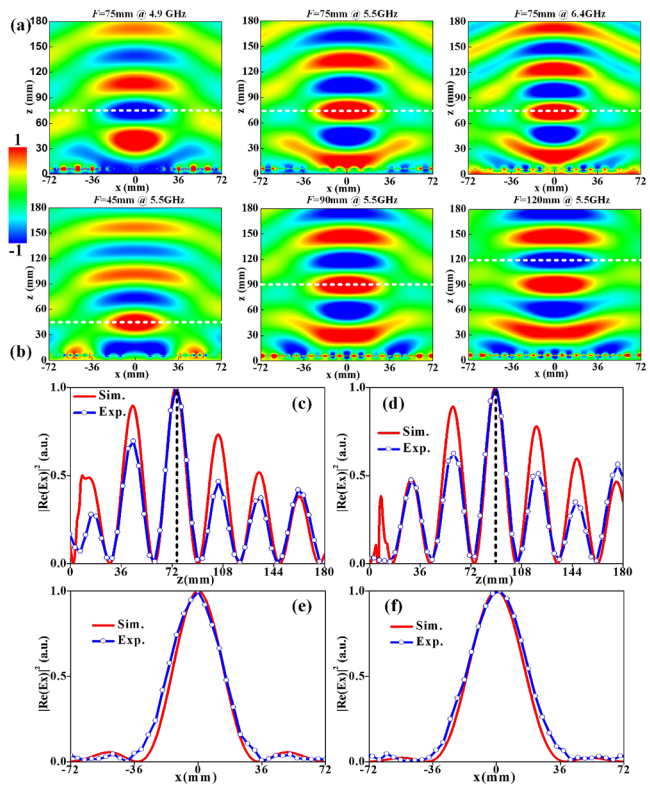

FIG. 5. FDTD simulated Re(E_x) field distributions for the (a) aberration-free lens (first row) with $F = 75$ mm at 4.9 GHz (left panel), 5.5 GHz (middle panel), and 6.4 GHz (right panel), respectively, and the (b) functionality-switchable lens (bottom row) with F varying from 45 mm to 120 mm at 5.5 GHz. ((c) and (d)) Comparison between simulated and measured field distributions along the z axis at x = 0 mm and ((e) and (f)) along the focal lines at z = 75 and 90 mm, for the tunable meta-lens with ((c) and (e)) $F = 75$ mm and ((d) and (f)) $F = 90$ mm at the frequency 5.5 GHz. Here, all fields are normalized against the peak values in the distributions.

reaches a maximum at the expected focal points in two different cases. The focal-spot size (half power beamwidth) was measured as 33 mm for the $F = 75$ mm case and increases slightly as F further increases. This is quite physical, since the small aperture size makes our meta-lens less efficient for long-focal-length imaging.

To sum up, we have established an active scheme to solve the dispersion-induced issues in passive meta-lenses and experimentally demonstrated the idea in the microwave regime. Adopting tunable meta-atoms involving varactor diodes controlled by external voltages, we can precisely control the phase profile of the constructed meta-lens and thus rectify the dispersion-induced distortions and conveniently change the focusing functionality. Such a concept was verified by both experiments and full-wave simulations, which are in perfect agreement with each other, based on a realistic meta-lens sample fabricated. Our approach can stimulate other exciting dynamically-switched and dispersion-compensated applications based on metasurfaces in the microwave regime.

This work was supported by National Natural Science Foundation China (Grant Nos. 61501499, 11474057, 61372034, 11674068, and 11404063), China Postdoctoral Science Foundation under Grant Nos. 2015M570323 and 2016T90337, MOE of China (Grant No. B06011), Shanghai Science and Technology Committee (Grant Nos. 16ZR1445200, 16JC1403100), and also Natural Science Foundation of Shaanxi Province under Grant No. 2016JQ6001.

[1]N. F. Yu, P. Genevet, M. A. Kats, F. Aieta, J.-P. Tetienne, F. Capasso, and G. Zeno, Science **334**, 333 (2011).
[2]N. Engheta, Science **334**, 317 (2011).
[3]X. Ni, N. K. Emani, A. V. Kildishev, A. Boltasseva, and V. M. Shalaev, Science **335**, 427 (2012).
[4]F. Aieta, P. Genevet, N. F. Yu, M. A. Kats, Z. Gaburro, and F. Capasso, Nano Lett. **12**, 1702 (2012).
[5]N. K. Grady, J. E. Heyes, D. R. Chowdhury, Y. Zeng, M. T. Reiten, A. K. Azad, A. J. Taylor, D. A. R. Dalvit, and H. T. Chen, Science **340**, 1304 (2013).
[6]N. F. Yu and F. Capasso, Nat. Mater. **13**, 139 (2014).
[7]S. L. Sun, K. Y. Yang, C. M. Wang, T. K. Juan, W. T. Chen, C. Y. Liao, Q. He, S. Y. Xiao, W. T. Kung, G. Y. Guo *et al.*, Nano Lett. **12**, 6223 (2012).
[8]Z. Li, E. Palacios, S. Butun, and K. Aydin, Nano Lett. **15**, 1615 (2015).
[9]Z. Zhang, Z. Tian, W. Yue, J. Gu, S. Zhang, J. Han, and W. Zhang, Adv. Mater. **25**, 4567 (2013).
[10]C. Pfeiffer, N. K. Emani, A. M. Shaltout, A. Boltasseva, V. M. Shalaev, and A. Grbic, Nano Lett. **14**, 2491 (2014).
[11]Z. C. Liu, Z. C. Li, Z. Liu, J. X. Li, H. Cheng, P. Yu, W. W. Liu, C. C. Tang, C. Z. Gu, J. J. Li *et al.*, Adv. Funct. Mater. **25**, 5428 (2015).
[12]F. Qin, L. Ding, L. Zhang, F. Monticone, C. C. Chum, J. Deng, S. T. Mei, Y. Li, J. H. Teng, M. H. Hong *et al.*, Sci. Adv. **2**, e1501168 (2016).
[13]S. L. Sun, Q. He, S. Y. Xiao, Q. Xu, X. Li, and L. Zhou, Nat. Mater. **11**, 426 (2012).
[14]J. Lin, M. J. P. Balthasar, Q. Wang, G. Yuan, N. Antoniou, X.-C. Yuan, and F. Capasso, Science **340**, 331 (2013).
[15]X. Chen, L. Huang, H. Muhlenbernd, G. Li, B. Bai, Q. Tan, G. Jin, C.-W. Qiu, S. Zhang, and T. Zentgraf, Nat. Commun. **3**, 1198 (2012).
[16]F. Aieta, P. Genevet, M. A. Kats, N. F. Yu, R. Blanchard, Z. Gahurro, and F. Capasso, Nano Lett. **12**, 4932 (2012).
[17]X. Ni, S. Ishii, A. V. Kildishev, and V. M. Shalaev, Light-Sci. Appl. **2**, e72 (2013).
[18]C. Pfeiffer and A. Grbic, IEEE Trans. Microwave Theory Tech. **61**, 4407 (2013).
[19]F. Monticone, N. M. Estakhri, and A. Alù, Phys. Rev. Lett. **110**, 203903 (2013).
[20]G. Spektor, A. David, B. Gjonaj, G. Bartal, and M. Orenstein, Nano Lett. **15**, 5739 (2015).
[21]X. Chen, M. Chen, M. Q. Mehmood, D. D. Wen, F. Y. Yue, C. W. Qiu, and S. Zhang, Adv. Opt. Mater. **3**, 1201 (2015).
[22]A. Pors, M. G. Nielsen, R. L. Eriksen, and S. I. Bozhevolnyi, Nano Lett. **13**, 829 (2013).
[23]M. Farmahini-Farahani and H. Mosallaei, Opt Lett. **38**, 462 (2013).
[24]F. Aieta, M. A. Kats, P. Genevet, and F. Capasso, Science **347**, 1342 (2015).
[25]X. Ni, A. V. Kildishev, and V. M. Shalaev, Nat. Commun. **4**, 2807 (2013).
[26]L. Huang, X. Z. Chen, H. Muhlenbernd, H. Zhang, S. M. Chen, B. F. Bai, Q. Tan, G. Jin, K. W. Cheah, and C.-W. Qiu *et al.*, Nat. Commun. **4**, 2808 (2013).
[27]Y. W. Huang, W. T. Chen, W. Y. Tsai, P. C. Wu, C. M. Wang, G. Sun, and D. P. Tsai, Nano Lett. **15**, 3122 (2015).
[28]G. Zheng, H. Mühlenbernd, M. Kenney, G. Li, T. Zentgraf, and S. Zhang, Nat. Nanotechnol. **10**, 308 (2015).
[29]P. Genevet, N. F. Yu, F. Aieta, J. Lin, M. A. Kats, R. Blanchard, M. O. Scully, Z. Gaburro, and F. Capasso, Appl. Phys. Lett. **100**, 013101 (2012).
[30]H. F. Ma, G. Z. Wang, G. S. Kong, and T. J. Cui, Sci. Rep. **5**, 9605 (2015).
[31]N. F. Yu, F. Aieta, P. Genevet, M. A. Kats, Z. Gaburro, and F. Capasso, Nano Lett. **12**, 6328 (2012).
[32]W. Luo, S. Xiao, Q. He, S. Sun, and L. Zhou, Adv. Opt. Mater. **3**, 1102 (2015).
[33]X. Yin, Z. Ye, J. Rho, Y. Wang, and X. Zhang, Science **339**, 1405 (2013).
[34]M. Kim, A. M. H. Wong, and G. V. Eleftheriades, Phys. Rev. X **4**, 041042 (2014).
[35]L. Liu, X. Zhang, M. Kenney, X. Su, N. Xu, C. Ouyang, Y. Shi, J. Han, W. Zhang, and S. Zhang, Adv. Mater. **26**, 5031 (2014).
[36]J. Zhao, Q. Cheng, J. Chen, M. Q. Qi, W. X. Jiang, and T. J. Cui, New J. Phys. **15**, 043049 (2013).
[37]T. Jiang, Z. Y. Wang, D. Li, J. N. Pan, B. Zhang, J. T. Huangfu, Y. Salamin, C. Z. Li, and L. X. Ran, IEEE Trans. Microwave Theory Tech. **60**, 170 (2012).
[38]H. Wakatsuchi, S. Kim, J. J. Rushton, and D. F. Sievenpiper, Phys. Rev. Lett. **111**, 245501 (2013).
[39]I. V. Shadrivov, P. V. Kapitanova, S. I. Maslovski, and Y. S. Kivshar, Phys. Rev. Lett. **109**, 083902 (2012).
[40]T. J. Cui, M. Q. Qi, X. Wan, J. Zhao, and Q. Cheng, Light-Sci. Appl. **3**, e218 (2014).
[41]B. O. Zhu, K. Chen, N. Jia, L. Sun, J. Zhao, T. Jiang, and Y. Feng, Sci. Rep. **4**, 4971 (2014).
[42]See www.skyworksinc.com for Skyworks Data Sheet, Skyworks Solutions, Inc.
[43]f_2 is also slightly tuned. However, since the varactor diode is connected the central bar of the "H" structure, it affects f_1 more significantly than on f_2.
[44]A. K. Iyer and G. V. Eleftheriades, IEEE Trans. Antennas Propag. **55**, 2746 (2007).
[45]H.-X. Xu, G.-M. Wang, M. Q. Qi, L. Li, and T. J. Cui, Adv. Opt. Mater. **1**, 495 (2013).